JOURNAL OF GEOPHYSICAL RESEARCH, VOL. 112, B01401, doi:10.1029/2005JB004244, 2007

Microplate model for the present-day deformation of Tibet

Wayne Thatcher[1]

Received 23 December 2005; revised 21 July 2006; accepted 25 August 2006; published 17 January 2007.

[1] Site velocities from 349 Global Positioning System (GPS) stations are used to construct an 11-element quasi-rigid block model of the Tibetan Plateau and its surroundings. Rigid rotations of five major blocks are well determined, and average translation velocities of six smaller blocks can be constrained. Where data are well distributed the velocity field can be explained well by rigid block motion and fault slip across block boundaries. Residual misfits average 1.6 mm/yr compared to typical one standard deviation velocity uncertainties of 1.3 mm/yr. Any residual internal straining of the blocks is small and heterogeneous. However, residual substructure might well represent currently unresolved motions of smaller blocks. Although any smaller blocks must move at nearly the same rate as the larger blocks within which they lie, undetected relative motions between them could be significant, particularly where there are gaps in GPS coverage. Predicted relative motions between major blocks agree with the observed sense of slip and along-strike partitioning of motion across major faults. However, predicted slip rates across Tibet's major strike-slip faults are low, only 5–12 mm/yr, a factor of 2–3 smaller than most rates estimated from fault offset features dated by radiometric methods as ~2000 to ~100,000 year old. Previous work has suggested that both GPS data and low fault slip rates are incompatible with rigid block motions of Tibet. The results reported here overcome these objections.

Citation: Thatcher, W. (2007), Microplate model for the present-day deformation of Tibet, *J. Geophys. Res.*, *112*, B01401, doi:10.1029/2005JB004244.

1. Introduction

[2] Collision of India with Eurasia during the past ~40 million years (Myr) has created the Himalayas, the Tibetan Plateau, and active faulting and crustal deformation that extends more than 2000 km into central Asia [*Molnar and Tapponnier*, 1975; *Burchfiel and Royden*, 1991; *Yin and Harrison*, 2000]. After decades of research and partisan debate there is still no consensus on how best to describe the widespread deformation occurring here and elsewhere on the continents. Two alternative end-member models have been proposed (Figure 1). At one extreme, in analogy with the global tectonic model of rigid plates, it has been suggested that actively deforming regions are comprised of blocks or microplates. Most deformation occurs along major block-bounding faults, with minor faulting but little internal deformation of the blocks themselves. This model has been advocated primarily by geologists who cite evidence for high (10–30 mm/yr) slip rates on the major strike-slip faults of Tibet [*Avouac and Tapponnier*, 1993; *Peltzer and Saucier*, 1996; *Replumaz and Tapponnier*, 2003; *Ryerson et al.*, 2006, and references therein]. At the opposite extreme, continental deformation is viewed as quasi-continuous, governed by the fluid-like solid-state flow of a viscous material. This model has been proposed primarily by geophysicists using laboratory measurements to constrain the ductile flow properties of Earth's lithosphere, its strong outer, ~100 km thick surface layer, and construct dynamical models of continental deformation [*England and McKenzie*, 1982; *Vilotte et al.*, 1982; *England and Molnar*, 1997b; *Flesch et al.*, 2001]. In this view, discrete slip in the brittle upper crust occurs on many faults with roughly comparable slip rates.

[3] It has been recognized for many years that Global Positioning System (GPS) data are likely to be ultimately decisive in distinguishing between block and continuum models, at least for describing present-day deformation [e.g., *McKenzie*, 1990; *Gordon and Stein*, 1992; *Thatcher*, 1995]. Nonetheless, both block models [e.g., *Le Pichon et al.*, 1995; *McCaffrey*, 2005; *McClusky et al.*, 2000; *Meade and Hager*, 2005; *Nyst and Thatcher*, 2004; *Thatcher et al.*, 1999; *L. M. Wallace et al.*, 2004] and continuum interpretations [e.g., *Chen et al.*, 2004b; *Flesch et al.*, 2000, 2001; *England and Molnar*, 2005; *Zhang et al.*, 2004] have been proposed to explain GPS observations in many regions of the deforming continents.

[4] However, as Figure 1 illustrates, the transition between block and continuum models is gradational rather than abrupt and the two converge as the number of faults increase and the block size decreases. Most researchers today would perhaps agree that the major unresolved issue is not which of the two extreme models is unconditionally correct, but how the observed deformation can be most usefully and simply described and which intermediate case is most appropriate. If a small number of blocks can explain

[1]U.S. Geological Survey, Menlo Park, California, USA.

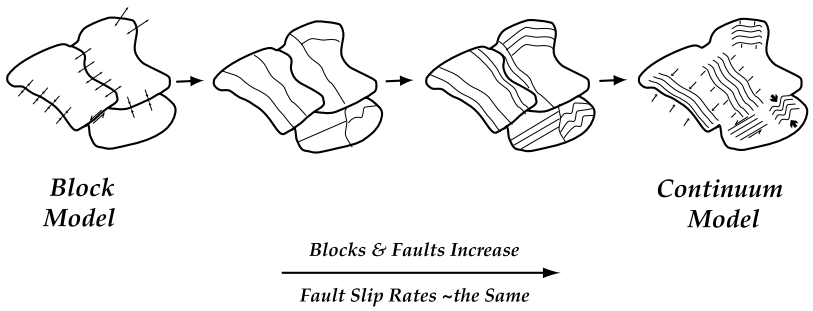

Figure 1. Schematic cartoon of end-member kinematic models for continental deformation with possible transitions from one to the other.

the first-order features of observed movements then continental deformation is more plate-like. If numerous blocks are required a continuum description is more useful. The distinction may also depend upon the scale of the problem being addressed and the precision required. Only a small number of blocks may be necessary to accurately describe first-order features on an intracontinental scale or local deformation with great precision. Many blocks may be needed to finely match observations at any scale. Here I address these issues by analyzing GPS data from Tibet.

[5] This paper is organized into five subsequent sections. First I show the observed GPS velocity field and describe its principal features. Next I define candidate blocks, determine their motions relative to Eurasia, and compare observed and predicted velocities. Predicted relative motions between the major blocks are then compared with geological constraints on the sense, partitioning, and rate of slip across Tibet's major faults. I then consider the strengths and limitations of the block model analysis and conclude with a summary of results and their implications for the kinematics and dynamics of continental deformation.

2. Observed GPS Velocity Field

[6] I analyze data from a recently published compilation of GPS space geodetic measurements from the Tibetan Plateau by *Zhang et al.* [2004]. They obtained velocities of points in Tibet relative to a stable Eurasia reference frame from episodic reoccupation of geodetic survey benchmarks since the early 1990s. The subset of these GPS velocities used in my study is shown in Figure 2, compared with the complete data set in Figure S1 and listed in the auxiliary material.[1] Here 349 of the 553 GPS site velocities obtained by Zhang et al. are used. Except as discussed below, all of the relevant Zhang et al. data have been used and no apparent outliers have been removed.

[7] To simplify my analysis and make the results more transparent I chose to eliminate regions where effects of elastic strain accumulation are large. Additional sites are also excluded where stations are sparse or velocities are not accurate enough to determine motions reliably; this includes 31 stations NE of the Haiyuan fault near the Ordos graben; 21 stations north of the eastern end of the Altyn Tagh fault (ATF); and six sites west of the Tarim Basin. 67 sites near the southern front of the Himalayas in northern India and Nepal are strongly affected by elastic strain accumulation, have been analyzed previously [*Cattin and Avouac*, 2000; *Chen et al.*, 2004a] and are not used here. Six sites near major faults within Tibet are eliminated for the same reason. I also exclude 71 sites SW of the Red River fault in Yunnan that show a complex velocity field due to slip across closely spaced faults and the motions of small blocks [*Wang et al.*, 1998; *Shen et al.*, 2005]. In principle, the effects of strain accumulation can be corrected for, but this usually involves assumptions about fault geometry and the transition between shallow locked (i.e., nonslipping) and deeper freely sliding fault segments that are seldom well known in Tibet. Rather than make uncertain corrections and introduce an additional layer of assumptions into the analysis, I choose to simply eliminate sites where these effects are evident or suspected. Retrospective examination of residuals verifies the correctness of these assumptions and confirms that the effects of elastic strain accumulation are small and can be neglected for the data I have analyzed.

[8] Figure 2 shows there is a general south-to-north decrease in velocity from 36–40 mm/yr in India to 5 mm/yr or less in the Gobi Ala Shan. About half, ~15–20 mm/yr, of this decrease occurs in northern India and Nepal and is due to the underthrusting of the Indian plate beneath the Himalayas. A comparable amount occurs within Tibet and is the subject of this paper.

[9] Visual inspection of GPS vectors in Figure 2 shows evidence that crustal blocks bounded by major strike-slip faults in eastern Tibet rotate clockwise (CW) about nearby rotation axes. This interpretation is most obvious for the block between the Haiyuan and Kunlun faults, where the arcuate, concave downward pattern of vectors suggest rotation relative to fixed Eurasia about a vertical axis (Euler pole) located ~1000 km to the south. In SE Tibet between

[1] Auxiliary material data sets are available at ftp://ftp.agu.org/apend/jb/2005jb004244. Other auxiliary material files are in the HTML.

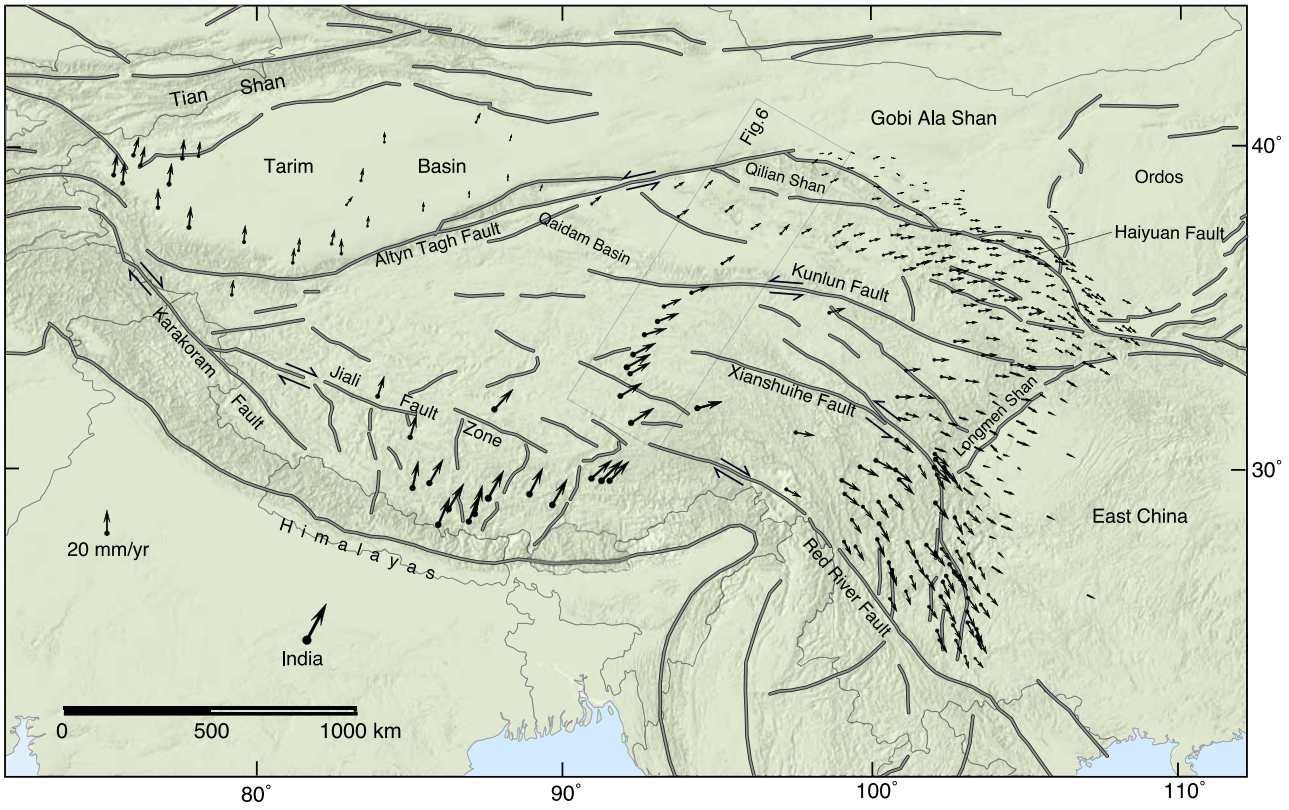

Figure 2. Tibet and surrounding regions, with GPS velocity vectors relative to stable Eurasia (to the north of map area). Velocity uncertainties are generally 1–2 mm/yr, so most error ellipses are illegible at this scale and are not plotted. Gray lines show active faults. Paired arrows show sense of slip on major strike-slip faults (except, to avoid clutter, for the Haiyuan fault, which is left lateral). Major faults and regions discussed in the text are labeled for reference. Rectangle shows location of profile for which observed and model-predicted velocities are plotted in Figure 6.

the Xianshuihe (XSH) and Red River faults the pattern of vectors also suggests CW rotation, here about an Euler pole located SW of this block. Rotation of the Tarim Basin about a pole located to the east has been previously documented [*Reigber et al.*, 2001] and is also evident. Though less obvious, the attuned eye may also see a hint in Figure 2 that the block between the Kunlun and XSH faults is rotating about an Euler pole to the south. Formal analysis described below confirms these hunches and quantifies the rotation of an additional block in central Tibet.

3. Data Analysis

[10] GPS data are sufficiently numerous and accurate to determine Euler vectors for five blocks and assess block rigidity by examining the misfit of model to data. Average translation velocities for six additional blocks can also be obtained. Establishing block boundaries is straightforward because major faults define most of the blocks. Elsewhere, as detailed below, choices are more subjective. Figure 3 shows the blocks used here. I describe the choice of boundaries from north to south with reference to Figures 2 and 3.

[11] 1. The northern boundary of the Qilian Shan (QS) block is defined by faults bounding the Gobi Alashan platform mapped by *Meyer et al.* [1998]. The southern boundary includes the Tanghenan Shan thrusts and the left-lateral strike-slip Haiyuan fault.

[12] 2. The NE Tibet (NET) block is bounded on the SW by the Qaidam basin, to the east by the SSE striking right-lateral Wenquan fault, and on the south by the eastern segment of the left-lateral strike-slip Kunlun fault.

[13] 3. The Qaidam basin (QB) block is bounded on the NW by the Altyn Tagh fault (ATF) and on the south by the Kunlun fault. Its SW boundary is uncertain: it may continue west from the Kunlun to the ATF as shown in Figure 2 or step south ~150 km to the Manyi fault, site of the 1997 M_w = 7.6 left-lateral strike-slip earthquake with 150 km of surface faulting.

[14] 4. The Tarim basin (TB) is well defined by major faults, those of the Tian Shan range on the north and the ATF on the south.

[15] 5. The Songpan (SP) block is bounded by the Kunlun fault on the north and the Xianshuihe (XSH) fault on the south. On the SE, following *Burchfiel* [2004] and *Shen et al.* [2005], I have defined the boundary not by the Longmen Shan but by an approximately ENE-WSW striking zone of high GPS velocity gradient ~100–200 km west of this mountain front. The lozenge-shaped region bounded by the SP block and the Longmen Shan moves at nearly the same velocity as east China (EC) and so I assume it is attached to the EC block. The ~500-km-long southwestern boundary is

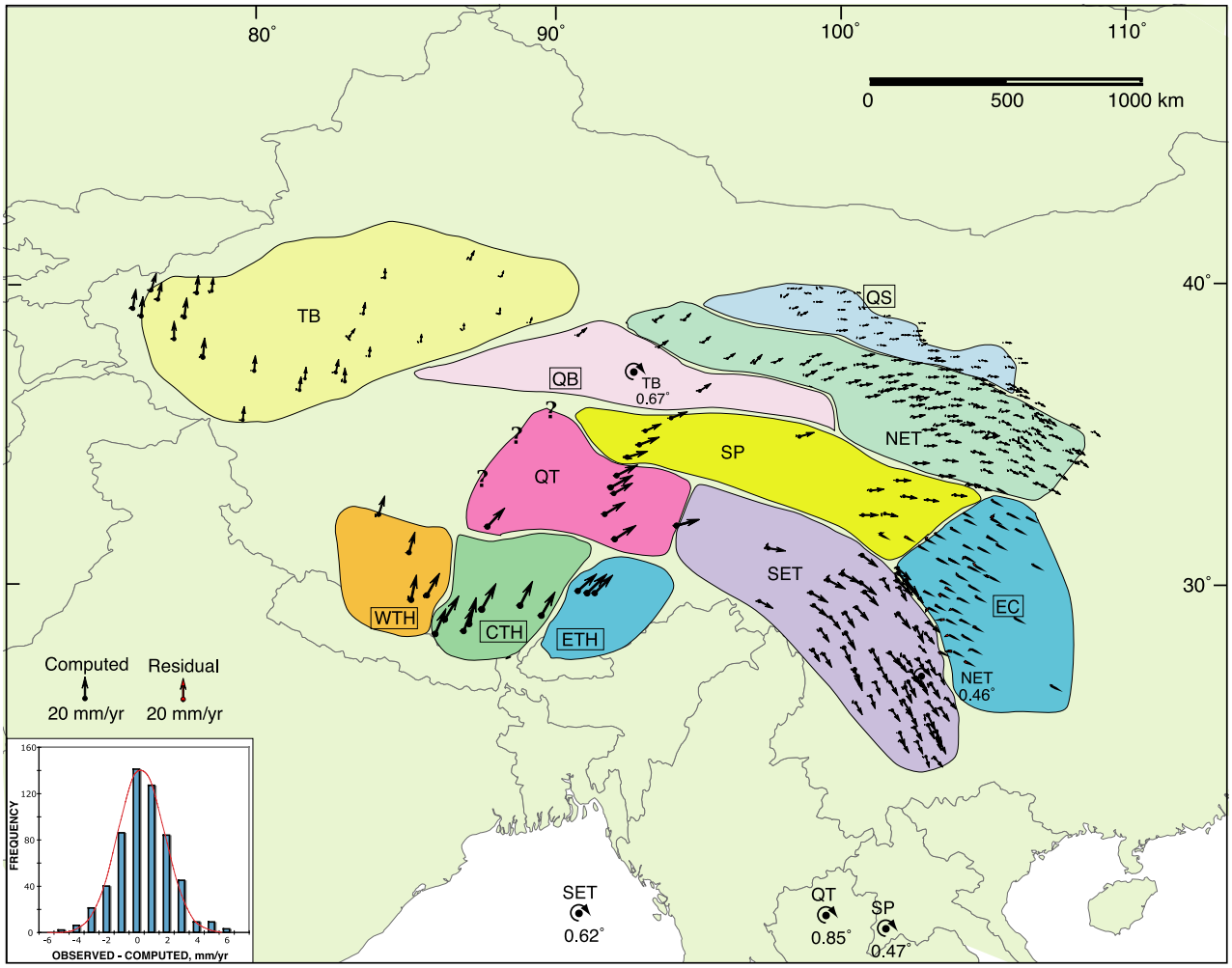

Figure 3. Observed velocity field (black arrows) and block model of Tibet. Blocks are color coded with abbreviated names as indicated. Smaller arrows show differences between observed and computed velocities (many are too small to be seen at true scale; these residuals are shown alone at an expanded scale in Figure 4). Inset shows histogram of residuals, which are fit well by a Gaussian distribution with mean of 0.4 and standard deviation of 1.6 mm/yr. Euler poles (rotation axes) and rotation rates (in degrees per million years) are shown for five blocks (NET, northeast Tibet; QT, Qiangtang; SET, southeast Tibet; SP, Songpan; TB, Tarim Basin). Average translation velocities relative to Eurasia are shown for six additional blocks whose abbreviated names are enclosed by rectangles (CTH, central Tibet Himalaya; EC, east China; ETH, eastern Tibet Himalaya; WTH, western Tibet Himalaya; QB, Qaidam Basin; QS, Qilian Shan). Block model parameters along with data and model fit statistics are listed in Tables 1 and 2.

problematic: I have continued it west of the XSH fault close to the Fenguo thrusts and Jinsha suture [*Meyer et al.*, 1998], near where en echelon strike-slip faults have also been suggested and strike-slip earthquake focal mechanisms have been obtained [*Molnar and Lyon-Caen*, 1989].

[16] 6. The Qiangtang (QT) block is bounded on the south by the discontinuous en echelon segments of the Jiali fault zone [*Armijo et al.*, 1989]. The western boundary shown in Figure 3 is extremely uncertain. There might well be several additional smaller blocks in western Tibet unconstrained by any GPS data. The eastern boundary of the QT block is rather arbitrarily located just to the east of a GPS station apparently on that block (J019; 31.9°N, 94.1°E); it could be as much as several hundred kilometers farther east.

[17] 7. The three blocks in southern Tibet (WTH, CTH, ETH) are separated by two major approximately N-S oriented normal faults that seems to bound groups of GPS sites with similar velocities [see also *Chen et al.*, 2004a].

[18] 8. GPS stations on the east China (EC) block east of the SP and SET blocks have been grouped together to estimate their average translation velocity with respect to Eurasia. This average velocity is quite consistent with rotation about the distant Euler pole estimated recently by *Shen et al.* [2005] using a more broadly distributed GPS data set from south and east China.

[19] 9. The SE Tibet (SET) block is bounded on the north by the XSH fault and on the east by its southerly continuation into the Xiaojiang fault. On the south the boundary is taken to be the Jiali and Red River faults, although the two

Table 1. Tibet Block Rotation Parameters

Block	Number of Stations	RMS S/N[a]	NRMS Misfit[b]	Latitude, °N	Longitude, °E	Rotation Rate,[c] deg/Myr
Tarim Basin (TB)	26	7.54	1.39	36.9 ± 0.2	93.4 ± 0.6	−0.67 ± 0.03
Songpan (SP)	16	8.21	1.69	18.2 ± 0.2	101.1 ± 0.04	−0.47 ± 0.01
Qiangtang (QT)	7	11.07	1.74	19.4 ± 2.3	99.6 ± 1.2	−0.85 ± 0.13
SE Tibet (SET)	72	12.15	1.96	19.7 ± 0.4	90.6 ± 0.5	−0.62 ± 0.03
NE Tibet (NET)	112	5.87	1.38	26.4 ± 0.4	102.4 ± 0.1	−0.46 ± 0.02

[a]RMS S/N is square root of sum of squares of observed velocity/uncertainty divided by number of observations.
[b]NRMS misfit is square root of sum of squares of (observed minus computed velocity)/uncertainty divided by number of observations minus degrees of freedom of model (equal to three Euler vector components).
[c]Counterclockwise rotation is positive.

faults are not continuous and may not be directly related to each other.

[20] Standard least squares analysis is used to determine the three Euler vector parameters (latitude and longitude of pole, rotation rate) for each block that best fit the two horizontal components of GPS velocity at each intrablock site. Rigid translations are estimated for the six additional, mostly smaller blocks within which data are either too sparse or too inaccurate to determine rotation parameters. Predicted velocities, misfit vectors, and Euler poles are shown in Figure 3. Listings of Euler parameters, their uncertainties, and data misfit statistics are included in Table 1. Corresponding parameters for block translations are given in Table 2. Figure 4 shows misfit vectors at a larger scale, and individual data fits are listed in auxiliary material. Figure 5 compares the observed velocities with the model-predicted small circles drawn about the Euler poles for the rotating blocks and the average translation directions for the other six blocks.

[21] The fit of model to data is generally very good. This can be examined visually in Figure 5 by comparing the observed vectors with the predicted block motions. Ideally, the velocity vectors within each rotating block should be tangent to small circles drawn about the Euler pole, with velocity magnitude given by the indicated rate in mm/yr. Velocities within each translating block should be constant and parallel to its average motion direction. The overall distribution of residuals is matched well by a Gaussian with a mean of 0.4 and standard deviation of 1.6 mm/yr (Figure 3 inset). The data used in the Euler vector determinations have RMS average signal-to-noise levels of 5.9 to 12.2. Individual normalized RMS misfits range from 1.4 to 1.9, corresponding to average residuals of ∼1.8 to 2.4 mm/yr. The noisier and less numerous data used to determine block translations are fit somewhat better (Table 2). The matches between model and data are as good or better than those typically obtained elsewhere in fitting GPS data to models of coseismic fault slip or interseismic deformation [*Feigl et al.*, 2002; *L. M. Wallace et al.*, 2004]. However, velocities are not all fit within their uncertainties, which average 1.3 mm/yr for each component. The small residual signals are probably due to true intrablock deformation and possible motions of smaller blocks, as well as unmodeled effects of lithospheric heterogeneity and elastic strain accumulation across block boundaries. The residuals show no simple, consistent, block-wide patterns and cannot be fit by a uniform strain rate field. Separate model runs that jointly invert for both Euler vector and uniform strain rate parameters produce small (3–13 nstrain/yr, 10^{-9}/yr) but statistically significant strain rates within some blocks. However, as Figure 4 suggests, any departures from block rigidity are unlikely to be usefully represented by a uniform strain rate field over the large block sizes used here, so I prefer applying the simpler model and examining departures from block rigidity using the residual pattern in Figure 4.

[22] The block model shown in Figures 3 and 5 is qualitatively similar to one proposed by *Replumaz and Tapponnier* [2003] (hereinafter referred to as RT) to model geologically inferred motions in central Asia over the past 5 Myr. The RT model in turn has significant similarities with earlier block models [*Avouac and Tapponnier*, 1993; *Peltzer and Saucier*, 1996]. Block structure adopted here differs from that used by RT in several regions where different criteria were used to define the blocks. For example, in NE Tibet the GPS data do not require subdivision into the several blocks suggested by RT, while in SE Tibet an additional block is needed. The TB, QB and SP blocks are similar to those defined by RT. Within the Tibetan Plateau, the blocks defined by RT rotate CW about Euler poles located to the south and east of Tibet. However, pole positions for blocks similar to those listed in Table 1 differ significantly, rotation rates are generally about a factor of 2 larger, and velocities predicted by the RT model are correspondingly 50 to 100% greater. As I discuss below,

Table 2. Tibet Block Translation Parameters

Block	Number of Stations	RMS S/N[a]	NRMS Misfit[b]	North Velocity, mm/yr	East Velocity, mm/yr
Qilian Shan (QS)	39	2.89	0.98	0.0 ± 1.0	4.3 ± 1.1
Qaidam Basin (QB)	3	9.11	1.01	6.8 ± 0.5	9.5 ± 1.0
West Tibet Himalaya (WTH)	3	12.65	1.57	22.2 ± 0.5	7.8 ± 3.1
Central Tibet Himalaya (CTH)	7	20.15	1.35	24.1 ± 0.8	11.5 ± 1.1
East Tibet Himalaya (ETH)	3	32.85	0.89	17.6 ± 0.4	18.5 ± 0.8
South China (SC)	56	32.21	1.35	−4.4 ± 1.2	7.2 ± 1.5

[a]RMS S/N is square root of sum of squares of observed velocity/uncertainty divided by number of observations.
[b]NRMS misfit is square root of sum of squares of (observed minus computed velocity)/uncertainty divided by number of observations minus degrees of freedom of model (equal to two translation vector components).

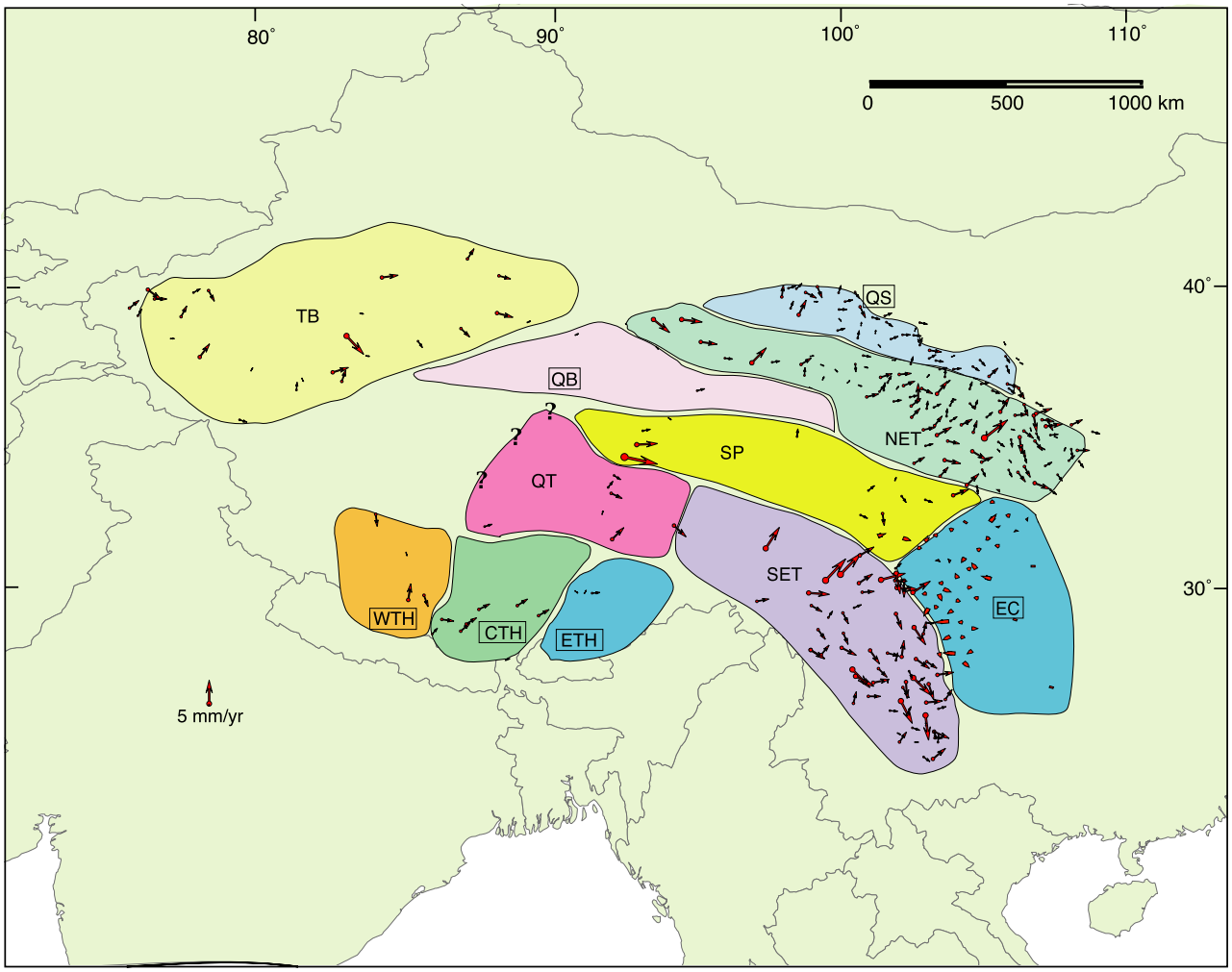

Figure 4. Misfit residuals from preferred block model plotted at 4 times the scale shown in Figure 3. Abbreviations are QT, Qiangtang; SET, southeast Tibet; SP, Songpan; TB, Tarim Basin; CTH, central Tibet Himalaya; ETH, eastern Tibet Himalaya; WTH, western Tibet Himalaya; EC, east China; QB, Qaidam Basin; QS, Qilian Shan.

these differences occur because the geological slip rates used by RT in building their model are a factor of 2 to 3 higher than the GPS estimates obtained here.

[23] Figure 4 shows suggestions of substructure at levels of as much as ~2–5 mm/yr that may represent heterogeneous internal straining or slow motion of smaller blocks. For example, residual velocities of 2–4 mm/yr in the western third of the NET block point eastward, suggesting this region could be a smaller independent block. Similarly, in the north central SET block, residuals of up to 5 mm/yr point NE, suggesting independent motion of this region. In addition, data distribution is inhomogeneous and sparse for several blocks. For example, the two clusters of vectors on the SP block are separated by more than 800 km. Although all SP data are fit acceptably with a single Euler vector, models with two or more blocks could also match the sparse data. In each of these examples the existing GPS data are insufficient to determine Euler vectors of blocks smaller than have been obtained here. However, this does not preclude a more complex block structure, and a recent study by *Shen et al.* [2005] of data from a newer, denser GPS network in Sechuan and Yunnan (SE half of SET block) demonstrates convincingly that three additional small blocks are needed there.

[24] Several previous studies of GPS data from Tibet have suggested that internal deformation of blocks is at least as important as slip along major faults in accounting for observed motions [*Wang et al.*, 2001; *Chen et al.*, 2004b; *Zhang et al.*, 2004]. These studies have each relied significantly on velocities from a quasi-linear array of GPS sites across Tibet. Such an array, which is oriented NNE, in the direction of India-Eurasia plate convergence, is outlined by the rectangular box in Figure 2. Corresponding velocity components parallel and perpendicular to the plate convergence direction are plotted versus latitude in Figure 6. As noted previously by others [*Wang et al.*, 2001; *Chen et al.*, 2004b; *Zhang et al.*, 2004] the velocity profiles lack the discrete offsets expected by block behavior and show a relatively smooth variation suggestive of continuum deformation. In particular, a straight line provides an excellent fit

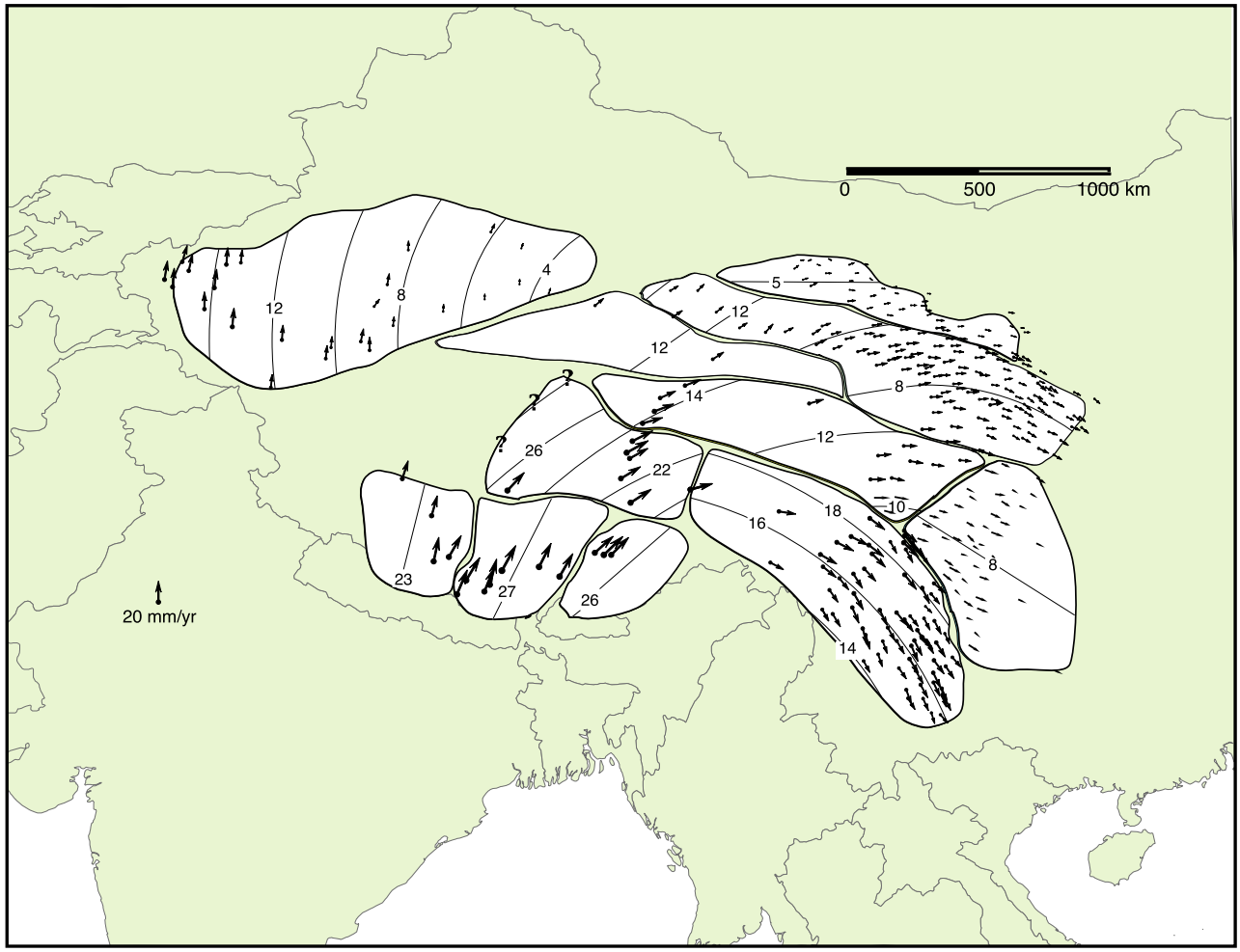

Figure 5. Observed GPS velocities, outlines of blocks used to fit observations, and predicted block motions (faint lines and arcs, with predicted velocities in mm/yr).

to the N20°E velocity component on this ~1100-km-long profile (see Figure 6a). The N110°E velocity component shows more variability and a linear fit is not as good (Figure 6b).

[25] Figure 6 shows that with the exception of a few outliers the block model provides a satisfactory fit to the profile data, but the match is not clearly superior to the linear fits. Indeed, the uniform strain rate model is much simpler and so might be considered the preferred interpretation for this profile. However, the block model itself relies largely on data from off the profile, where block rotation and translation effects are the dominant signal and a uniform strain rate field is clearly inappropriate.

4. Comparison With Geological Constraints

[26] Given the estimated motions of individual blocks in Tables 1 and 2 the relative motions across the block boundaries are uniquely determined, and these predicted velocities provide quantitative estimates of the rate and sense of slip across major faults. The orientation of the relative motion vector also constrains partitioning between fault-parallel and fault-normal deformation that may occur across the block boundary. Figure 7 shows the predicted relative velocities across boundary segments where GPS data distribution is satisfactory and constraints on block motions appear to be good. Geological estimates of late Quaternary/Holocene fault slip rates and structural studies of the style and partitioning of slip provide standards against which to measure the block model predictions.

4.1. Sense and Partitioning of Fault Motion

[27] In general the block model correctly predicts the sense of motion across the major strike-slip faults of Tibet as well as the partitioning and along-strike variation of relative motion. Slip on the Altyn Tagh and Kunlun faults is almost purely left lateral and shows little along strike variation. Small amounts of fault-normal compression might well be expected near the Kunlun Shan and the Altyn Shan ranges, which lie immediately to the north of these strike-slip faults [*Meyer et al.*, 1998]. However, GPS data constrain only rigid translation of the Qaidam block, and any along-strike variations in fault-normal velocity depend on likely but unknown velocity gradients due to rotation within the Qaidam block.

[28] On both the northern and southern boundaries of the NET block the predicted relative motions accord well with geological studies of *Meyer at al.* [1998]. Between the NET

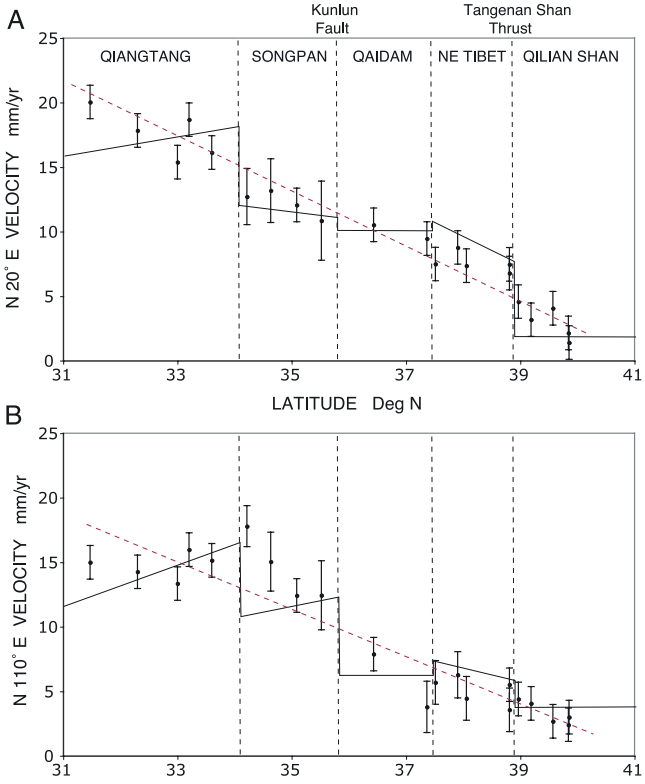

Figure 6. Observed and predicted GPS velocities along 1100-km-long, NNE oriented transect across central Tibet (see rectangle in Figure 2). Velocity components are plotted parallel (N20°E) and perpendicular (N110°E) to the average India-Eurasia convergence direction as a function of latitude. Observed velocities (dots) include one standard deviation error bars. Red dashed lines show linear fits to the two velocity components. Faint solid lines are predictions of the block model shown in Figure 3. Vertical dashed lines show approximate locations of block boundaries, with block names indicated. Kunlun fault and Qilian Shan frontal thrust (Tanghenan Shan) are shown for reference.

and the QS blocks, motion is nearly pure fault-normal convergence across the thrusts of the Tanghenan Shan; it becomes increasingly oblique farther east, and grades into purely left-lateral strike slip across the Haiyuan fault. Left-lateral strike-slip motion occurs across the eastern ~500 km of the Kunlun fault. Similar agreement is found on the boundary between the Qaidam basin and NE Tibet. Relative motions are negligible in the west, where mapped faults are short and ranges subdued; convergence increases toward the ESE as thrusts become more continuous and ranges grow; motions are nearly pure right-lateral strike slip across the NNW-SSE striking Wenquan fault, which bounds the QB block on the SE.

[29] A recent study of late Cenozoic deformation along the Wenquan fault [*Wang and Burchfiel*, 2004] found evidence for left-lateral slip at an average rate of ~4 mm/yr, in good agreement with the GPS results presented here. This same geological study suggested strong CW rotation of the Qaidam block, with convergence on its northern boundary increasing westward, opposite to that inferred here (Figure 7). However, only a small number of GPS sites currently determine the average translation of the QB block. Better GPS constraints on the rotation of this block are needed to determine its motion relative to the NET block and shed further light on the apparent discrepancy between the geologic and space geodetic results.

[30] Relative motion across the boundary between the QT and SP blocks is left lateral with a reverse component that increases to the WNW. No single major fault has been identified near this postulated boundary. However, earthquake fault plane solutions consistent with left-lateral strike slip on approximately E-W oriented faults occur in the region [*Molnar and Lyon-Caen*, 1989] and west and WNW striking thrust faults have been mapped as well [*Meyer et al.*, 1998].

[31] Several features of the predicted relative motions in SE Tibet are unexpected, and if true would be surprising. Although the predicted motion across the XSH fault between the SP and SET blocks is properly left lateral, nearly equal amounts of fault-normal extension are also predicted along the SP-SET boundary. Earthquake fault plane solutions show normal faulting just north of this segment of the XSH [*Molnar and Lyon-Caen*, 1989], but the extensional axes are fault-parallel rather than fault normal. As mentioned previously, misfit vectors for six stations lying to the south of the XSH fault in this region are approximately fault normal and as large as 5 mm/yr (see Figures 3 and 5); if regionally representative, such motions would negate much or all of the model-predicted extension. Introduction of a smaller, eastward moving block bounded on the east by an approximately north-south oriented strike-slip fault near 99°E could remove this fault-normal extension across the XSH between ~95° and 100°E, but not enough data currently exist to define its motion. However, farther SE, *Shen et al.* [2005] have sufficient new data to justify adding a subblock between the XSH and the subparallel Litang fault ~150 km south of it, resulting in pure strike slip on the XSH and left-lateral transtension across the Litang fault. Along the ~600-km-long boundary between the SET and EC blocks, predicted motions across the XSH and related faults is purely right lateral as expected.

[32] The predicted motion on the approximately N-S oriented boundary between the QT and SET blocks is right-lateral strike slip, and there are no mapped faults of this orientation in the region. GPS data distribution is sparse near this block boundary and within the western half of the SE Tibet block, so the actual geometry may be different and/or more complex than has been sketched in Figures 3, 5, and 7.

[33] As mentioned earlier, the chosen boundary between SP and EC blocks is oriented ENE-WSW and lies 100–2000 west of the Longmen Shan. This boundary lies near no identified major fault and is defined solely by a conspicuous change in the orientation and magnitude of GPS vectors (see Figures 2, 3, and 5). Predicted relative motion across this boundary is almost purely right lateral strike slip at a rate of 7 mm/yr.

4.2. Discrepancies Between Geological and GPS Slip Rate Estimates

[34] Despite the generally good agreement between geologically observed and GPS predicted orientations of interblock relative motion, Figure 7 shows that the fault slip

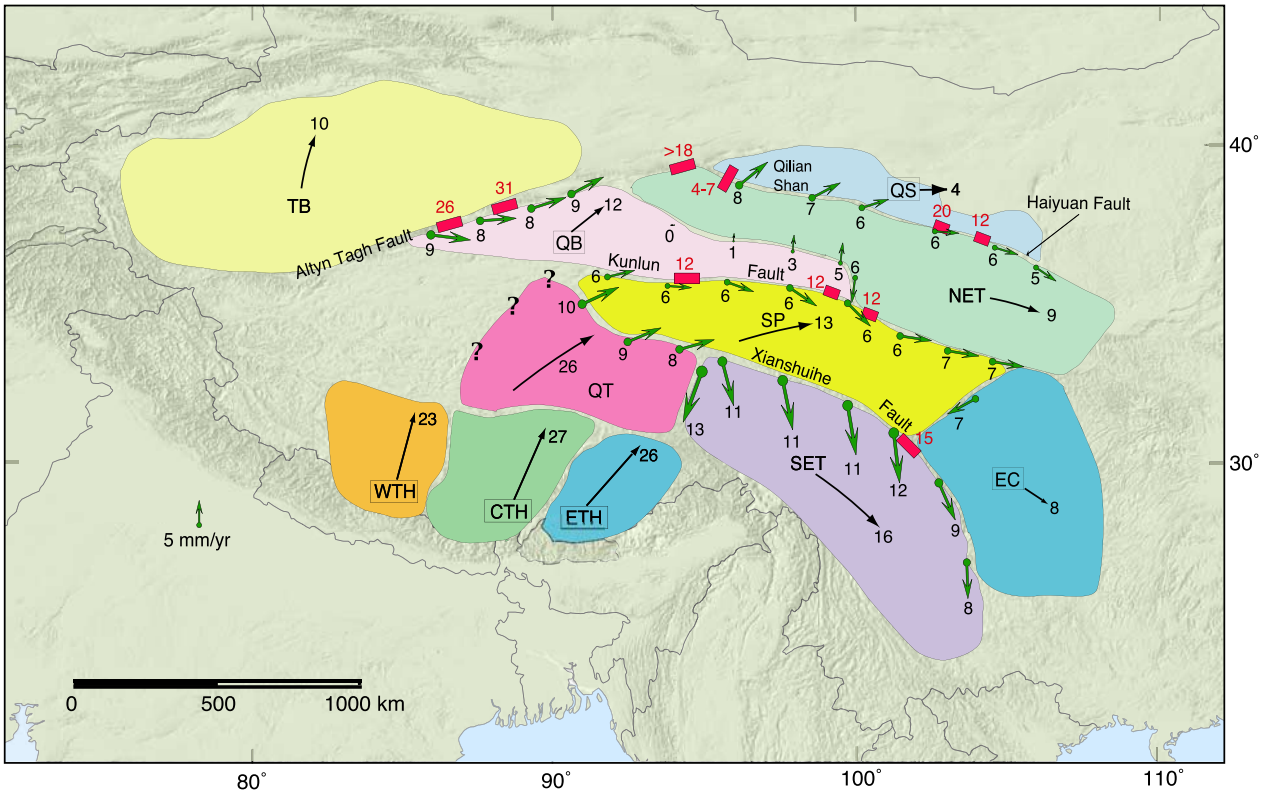

Figure 7. Predicted interblock velocities (thicker green arrows with numbers), with average block velocities relative to Eurasia (thinner black arrows) and geologically estimated slip rates (red numerals). All rates are in mm/yr. Blocks are color coded with names abbreviated as in Figure 3. The convention on interblock vectors is to show the motion of the southern block relative to its northern neighbor, or the eastern block relative to its western mate. Typical rates of motion (relative to Eurasia) near the centers of five rotating blocks are shown by arcs drawn from each of their Euler poles, with arc length proportional to velocity and arrowheads indicating the sense of rotation. The abbreviated names of five additional rigidly translating blocks are enclosed by faint rectangles. Their translation velocities relative to Eurasia are shown as thin straight arrows. Red rectangles show locations of sites where geological estimates of fault slip rate have been obtained by radiometric dating [*Ryerson et al.*, 2006; *Allen et al.*, 1991]; red numerals give the late Pleistocene-Holocene slip rates.

rates disagree significantly. The discrepancy is of the same order as that described previously using space geodetic data from the ATF [*K. Wallace et al.*, 2004] and Karakoram fault [*Wright et al.*, 2004]. Figure 7 shows that rates constrained by the GPS-based block model are 2 to 3 times smaller than most geologic estimates: ATF 8–9 mm/yr (GPS) versus 18–31 mm/yr (geologic); Kunlun (6–7 versus 12 mm/yr); Haiyuan (5–6 versus 12–20 mm/yr). Curiously, the geologic rate estimate of 4–7 mm/yr for reverse fault slip across the Tangenan Shan [*Van der Woerd et al.*, 2001] is in acceptable agreement with the block model estimate of 8 mm/yr convergence across this range front. The block model estimate of 12 mm/yr across the northern XSH fault is also consistent with slip rates bounding 15 ± 5 mm/yr estimated by radiocarbon dating at a number of localities in the same region [*Allen et al.*, 1991]. The origin of the slip rate discrepancy is contentious and currently unresolved.

4.3. GPS Estimates of Fault Slip Rates

[35] The GPS measurements span ~10 years or less, and presumed steady state velocities could be contaminated by poorly constrained effects of episodic [e.g., *Dragert et al.*, 2001] or transient deformation [e.g., *Hetland and Hager*, 2003]. However, deformation episodes observed elsewhere are spatially localized and it would be unprecedented for such an episode (or a comparable interval of retarded motions) to simultaneously affect different block-bounding faults up to 1000 km apart. Detectible postseismic deformation transients can continue for many decades after earthquakes of M7 or greater [e.g., *Hetland and Hager*, 2003]. The transients will tend to concentrate high-velocity gradients near the causative fault early in the earthquake cycle and spread them more broadly later in the cycle [*Thatcher*, 1983; *Thatcher and Rundle*, 1984]. This late cycle broadening could in principle lead to underestimation of fault slip rate, but should be revealed by low-velocity gradients that extend as much as several hundred km into the blocks. Furthermore, this effect is relatively subtle, will not significantly influence velocities farther from the fault, and by itself seems unlikely to explain the large slip rate discrepancy.

[36] The fault slip rates obtained here from the GPS velocity field are intrinsic to the data themselves and generally depend only weakly on the rigid block assumption. For example, *England and Molnar* [2005] used a completely independent analysis of central Asian GPS data and matched it to a smooth, quasi-continuous velocity field. Even with this very different initial assumption they found rates of relative motion across fault-spanning triangles of their model grid that are very similar to those obtained here (compare Figure 7 of this paper with Figure 17 of *England and Molnar* [2005]). As is discussed below in section 5, the largest limitation of the GPS data is its incomplete spatial coverage, particularly in central and western Tibet. However, the GPS data itself shows low-velocity gradients across Tibet's major faults, and if present-day slip rates are actually as high as suggested by the geologic interpretations the GPS data show no evidence of this.

4.4. Geologic Slip Rate Estimates

[37] The geologic slip rate estimates rely largely on surface exposure age dates of river terraces or glacial moraines offset by faulting (see review by *Ryerson et al.* [2006]). A series of recent papers that use surface exposure age dating methods to estimate slip rates on the Karakoram fault illustrate current problems and highlight differences in interpretation of available data [*Brown et al.*, 2002, 2005; *Chevalier et al.*, 2004, 2005].

[38] Strengths in the *Ryerson et al.* [2006] group's interpretation of high geologic slip rates include (1) identification of regionally correlative surfaces whose exposure age dates correspond to major climatic fluctuations independently constrained by oxygen isotope methods; (2) strong temporal clustering of dates obtained on individual terrace surfaces and moraines offset by faulting in a variety of locales along the ATF and elsewhere; and (3) linearity of age versus offset plots for both the Kunlun fault and ATF over measured ages ranging from as little as a few thousand years to as much as several hundred thousand years.

[39] However, several consistent biases in dating the time offset began accumulating on faulted features, although recognized by *Ryerson et al.* [2006] were not fully accounted for in assessing uncertainties in their derived slip rates. First, offset fluvial terrace risers furnish both a maximum and a minimum slip rate estimate. In the Tibet work it is usually assumed that offset of a terrace riser separating two surfaces (T1 and T2 say) does not begin accumulating until the lower (younger) terrace surface T1 has been abandoned and the river is no longer actively eroding that surface. This assumption provides a maximum slip rate estimate. However, this assumption could be violated if offset began accumulating prior to T1 abandonment. If instead it is assumed offset accumulated from the date of T2 abandonment, a minimum slip rate is obtained. Since these two estimates often differ by factors of 2 to 3, the lower bound is generally consistent with the GPS slip rate estimates, at least on the ATF. This issue has been recently investigated for the Cherchen He site on the ATF, where it is argued on geomorphic grounds that the lower bound rate of 9 ± 2 mm/yr is the most appropriate geologic slip rate estimate [*Cowgill*, 2006]. Second, the youngest surface age dates on the T1 terrace are invariably taken to date the abandonment of that surface. This assumption could be violated if the new active channel (T0 say) had its banks overtopped by a rare flood, depositing anomalously young material on T1. The assumption again leads to a potential bias toward high slip rates. Third, any shielding of the dated surface samples will bias measured ages too young and lead to an overestimate of slip rate. Examples include episodic loess burial and subsequent reexhumation and spallation of large boulders. The latter is likely to be important only for ages greater than $\sim$50 ka.

[40] Given presently available information it is perhaps equally hard to prove or to dismiss the importance of the consistent biases described above. Better understanding of the origin and evolution of fluvial terrace sequences and glacial moraines would contribute to placing the geological slip rate estimates in their appropriate geomorphic context and establish the degree to which geological and GPS slip rate estimates are truly inconsistent.

5. Strengths and Limitations of Block Model

[41] The block model proposed here has both strengths and shortcomings. Choosing candidate blocks largely bounded by major faults should not be controversial, and with this choice of boundaries the GPS data are satisfied by a model in which the blocks are largely rigid and rotate about extremely well constrained Euler poles (see Table 1). Any internal straining of the blocks is heterogeneous and small, but misfits to the model do not preclude local strain rates as high as $\sim$10–20 nstrain/yr (10^{-9}/yr) or faults slipping as much as $\sim$2–6 mm/yr. The relative motion between the blocks agrees with expectations based on structural mapping of active faults located at or near block boundaries, but predicted rates of slip are generally considerably less than those obtained by radiometric dating of offset fault features.

[42] Gaps in GPS data coverage (see Figures 2, 3, and 5) produce the largest model uncertainties. Significant portions of the QT, QB, SP and SET blocks are poorly sampled. In particular, there are only a few GPS stations in central and western Tibet between the Altyn Tagh and Jiali faults, so much of the motion of the QT and QB blocks is unconstrained. If the QT block were to include most of western Tibet, its western edges should be moving $\sim$35 mm/yr NE relative to Eurasia, implying high slip rates on the western portions of the Kunlun, Altyn Tagh, Jiali, and Karakoram faults. However, the region might well be comprised of several smaller blocks separated by strike-slip or normal faults. In southern Tibet, approximately E-W extension on approximately N-S grabens causes block translation velocities to decrease somewhat from east to west and have increasingly more northward orientations (see Figure 7). If western Tibet mimicked this behavior, significantly lower slip rates would be required on the major strike-slip faults located there.

[43] Block models for Tibet like that proposed here are by no means new, but for several reasons they have long been controversial. First, the geological estimates of high slip rates have themselves been controversial [*England and Molnar*, 1997a], and these rates have been used in the past to constrain block models [*Avouac and Tapponnier*, 1993; *Peltzer and Saucier*, 1996; *Replumaz and Tapponnier*, 2003]. This has led to the tacit assumption that the block

models are not viable if the fault slip rates are significantly less than the high geological estimates. Indeed, the low slip rates estimated by space geodetic methods have been used to argue that continuum models should be preferred [*K. Wallace et al.*, 2004; *Wright et al.*, 2004]. Second, analysis of the increasing volume of space geodetic data that has become available from Tibet over the past 5 years has generally been interpreted in favor of continuum models or those in which intrablock deformation is as important as slip on major faults [*Zhang et al.*, 2004; *Wang et al.*, 2001; *Chen et al.*, 2004b; *K. Wallace et al.*, 2004; *Wright et al.*, 2004]. My analysis suggests that both the GPS data and the low fault slip rates it implies are quite compatible with block motions in Tibet. A recent independent analysis of the Tibetan GPS data reaches this same conclusion [*Meade*, 2007].

6. Summary and Discussion

[44] GPS measurements uniquely quantify present-day Tibetan deformation that can be simply and usefully described by the relative motions of 11 quasi-rigid blocks and fault slip across block boundaries. Irregular GPS station distribution and large gaps in coverage produce the largest model uncertainties. Internal deformation of blocks, revealed by misfits to a model that assumes block rigidity, is small but apparently systematic. These residuals may represent unresolved motions of smaller blocks moving at slightly different rates or directions than the larger blocks within which they lie.

[45] Slip rates on Tibet's major strike-slip faults inferred from the GPS block modeling are systematically a factor of 2 to 3 lower than estimates based on surface exposure age dating of offset features [e.g., *Ryerson et al.*, 2006]. Previous analyses of space geodetic data from the Altyn Tagh and Karakoram faults first highlighted this discrepancy [*K. Wallace et al.*, 2004; *Wright et al.*, 2004] and results reported here extend it to the Kunlun and Haiyuan faults as well as additional portions of the Altyn Tagh fault. Although it has been suggested that differences between geologic and GPS estimates may reflect a temporal change in fault slip rates during the past ~2–100 kyr [e.g., *Chevalier et al.*, 2004], the systematic nature of the disagreement makes it seem unlikely this could be a plateau-wide phenomenon. The average convergence rate of 35–40 mm/yr between India and Eurasia has not changed significantly during the past ~3 Myr [*Gordon et al.*, 1999; *Sella et al.*, 2002] and any speed up or slow down in the relative motion between these large plates over shorter timescales is dynamically implausible. Therefore, if some faults within the deforming zone of Tibet were moving faster than current geodetically estimated rates in the geologically recent past, others must have been moving more slowly in order to preserve a constant India-Eurasia convergence rate. However, although geologic slip rates are now available on all the major faults in the India-Eurasia collision zone, none have been reported that are anomalously low relative to the GPS estimates.

[46] Although the concepts and rules of global plate kinematics can be applied to provide a first-order description of the current deformation of Tibet, continental tectonics differs from global plate tectonics in important ways, some of which remain controversial and are topics of ongoing research. The implications of the block models for the kinematics and dynamics of continental deformation are significantly dependent on (1) block rigidity; (2) whether or not the blocks and their bounding faults are geologically long-lived tectonic features; (3) how many blocks are needed to adequately describe observed deformation; and (4) how deeply into the continental lithosphere discrete block structures extend. In what follows I discuss each of these issues in turn.

[47] The rigidity of the blocks inferred from GPS data analysis remains uncertain. The occurrence of large earthquakes and young active faults in block interiors provides obvious evidence of departures from perfect rigidity. Misfits of GPS velocities to simple block models supply quantitative constraints and suggest that internal deformation is second order compared with straining at block boundaries. However, very small differences in rates and orientations of GPS velocity vectors can translate into significant intrablock deformation and fault slip. Consequently, very dense networks, high measurement precision, and very complete coverage are necessary to precisely bound such deformation and uncover any subblock structure.

[48] The longevity of crustal blocks can be constrained by geologically measurable internal deformation and the history of slip on bounding faults. The Tarim basin has long been a stable block surrounded by belts of intense deformation. Although evidence elsewhere on the Tibetan Plateau is less clear, Cenozoic shortening has occurred in several regions of the plateau that currently appear block-like [*Yin and Harrison*, 2000]. Determining late Quaternary/Holocene fault slip rates, obtaining cumulative offsets of older geologic markers, and dating the onset of sedimentation or deformation often places useful limits on the time interval over which a major fault has slipped at recent rates. Near the eastern margin of the Tibetan Plateau these methods have been used to suggest that major faults there have been active no more than 4–8 Myr [*Zhang et al.*, 1990; *Burchfiel et al.*, 1995; *Wang et al.*, 1998]. On the other hand, the Altyn Tagh fault may have been active for much longer if the apparent ~550 km offset of a late Paleozoic magmatic belt is a reliable measure of cumulative Cenozoic fault slip [*Peltzer and Tapponnier*, 1988; *Yin and Harrison*, 2000]. The strength of the evidence for block integrity and fault slip history will determine how confidently current movement patterns can be extrapolated into the geologic past in Tibet and elsewhere [e.g., *Replumaz and Tapponnier*, 2003].

[49] As mentioned earlier, the distinction between block and continuum models becomes blurred as block size decreases and slip rates on bounding faults become comparable (Figure 1). My own view is that block models are the preferred kinematic description of surface deformation and large GPS data sets unless it can be shown that so many blocks are required that a smooth, continuum description is a more economical way of summarizing observed movements. Even if this were so, block models would continue to be important in quantifying local tectonics, because continuum models inevitably smear out the discrete slip occurring across major faults.

[50] However, deformation at depth in the ductile lithosphere might well be considerably more continuous than it is at the surface. This will be especially likely where many

faults with comparable slip rates cut the surface into blocks with dimensions equal to or less than the average lithospheric thickness of ~100 km [e.g., *England and Houseman*, 1988; *England and Molnar*, 1997a]. Indeed, "GPS blocks" may extend no deeper than the base of the seismogenic upper crust (~20 km) if a ductile lower crust decouples near surface motions from the underlying mantle [e.g., *Zhao and Morgan*, 1987; *Bird*, 1991; *Royden et al.*, 1997; *Clark and Royden*, 2000]. Alternatively, if the major block-bounding faults extend into the lithospheric mantle [e.g., *Tapponnier et al.*, 2001], perhaps as weak, localized ductile shear zones, the surface kinematics will have a more important influence on the dynamics of continental deformation.

[51] **Acknowledgments.** Advice on computations by W. C. Hammond and with graphics by Serkan Bozkurt is gratefully acknowledged. Reviews by R. Burgmann, B. C. Burchfiel, and N.Okaya and comments by Z. K. Shen and A. Yin were extremely helpful. Careful reviews by J. C. Savage and J. R. Murray resulted in considerable improvement to an earlier version of this manuscript. I am particularly indebted to T. C. Hanks for his perceptive comments on the strengths and limitations of the published geological estimates of slip rates on Tibet's major faults.

References

Allen, C. R., Z. Luo, H. Qian, X. Wen, H. Zhou, and W. Huang (1991), Field study of a highly active fault zone: The Xianshuihe fault of southwestern China, *Geol. Soc. Am. Bull.*, *103*, 1178–1199.

Armijo, R., P. Tapponnier, and H. Tonglin (1989), Late Cenozoic right-lateral strike-slip faulting in southern Tibet, *J. Geophys. Res.*, *94*, 2787–2838.

Avouac, J.-P., and P. Tapponnier (1993), Kinematic model of active deformation in central Asia, *Geophys. Res. Lett.*, *20*, 895–898.

Bird, P. (1991), Lateral extrusion of lower crust from under high topography, in the isostatic limit, *J. Geophys. Res.*, *96*, 10,275–10,286.

Brown, E. T., R. Bendick, D. L. Bourlès, V. Gaur, P. Molnar, G. M. Raisbeck, and F. Yiou (2002), Slip rates of the Karakoram fault, Ladakh, India, determined using cosmic ray exposure dating of debris flows and moraines, *J. Geophys. Res.*, *107*(B9), 2192, doi:10.1029/2000JB000100.

Brown, E. T., P. Molnar, and D. L. Bourles (2005), Comment on "Slip-rate measurements on the Karakoram fault may imply secular variations in fault motion", *Science*, *309*, 1326.

Burchfiel, B. C. (2004), New technology; new geological challenges, *GSA Today*, *14*, 4–9.

Burchfiel, B. C., and L. H. Royden (1991), Tectonics of Asia 50 years after the death of Emile Argand, *Ecol. Geol. Helv.*, *84*, 599–629.

Burchfiel, B. C., Z. Chen, Y. Liu, and L. H. Royden (1995), Tectonics of the Longmen Shan and adjacent regions, *Int. Geol. Rev.*, *37*, 661–735.

Cattin, R., and J.-P. Avouac (2000), Modeling mountain building and the seismic cycle in the Himalaya of Nepal, *J. Geophys. Res.*, *105*, 13,389–13,407.

Chen, Q., J. T. Freymueller, Z. Yang, C. Xu, W. Jiang, Q. Wang, and J. Liu (2004a), Spatially variable extension in southern Tibet based on GPS measurements, *J. Geophys. Res.*, *109*, B09401, doi:10.1029/2002JB002350.

Chen, Q., J. T. Freymueller, Q. Wang, Z. Yang, C. Xu, and J. Liu (2004b), A deforming block model for the present-day tectonics of Tibet, *J. Geophys. Res.*, *109*, B01403, doi:10.1029/2002JB002151.

Chevalier, M.-L., F. J. Ryerson, P. Tapponnier, R. C. Finkel, J. Van der Woerd, L. Haibing, and L. Qing (2004), Slip-rate measurements on the Karakoram fault may imply secular variations in fault motion, *Science*, *307*, 411–414.

Chevalier, M.-L., F. J. Ryerson, P. Tapponnier, R. C. Finkel, J. Van der Woerd, L. Haibing, and L. Qing (2005), Response to comment on "Slip-rate measurements on the Karakoram fault may imply secular variations in fault motion", *Science*, *309*, 1326.

Clark, M. K., and L. H. Royden (2000), Topographic ooze: Building the eastern margin of Tibet by lower crustal flow, *Geology*, *28*, 703–706.

Cowgill, E. (2006), Riser reconstructions and their impact on secular variation in rates of strike-slip faulting: Revisiting the Cherchen He site along the Altyn Tagh fault, *Earth Planet. Sci. Lett*, in press.

Dragert, H., K. Wang, and T. S. James (2001), A silent slip event on the deeper Cascadia subduction interface, *Science*, *292*, 1525–1528.

England, P., and G. A. Houseman (1988), The mechanics of the Tibetan Plateau, *Philos. Trans. R. Soc. London, Ser. A*, *326*, 301–320.

England, P., and D. McKenzie (1982), A thin viscous sheet for continental deformation, *Geophys. J.R. Astron. Soc.*, *70*, 295–321.

England, P., and P. Molnar (1997a), The field of crustal velocity in Asia calculated from Quaternary rates of slip on faults, *Geophys. J. Int.*, *130*, 551–582.

England, P., and P. Molnar (1997b), Active deformation of Asia: From kinematics to dynamics, *Science*, *278*, 647–650.

England, P., and P. Molnar (2005), Late Quaternary to decadal velocity fields in Asia, *J. Geophys. Res.*, *110*, B12401, doi:10.1029/2004JB003541.

Feigl, K., F. Swarti, H. Vadon, S. McClusky, S. Ergintav, P. Durand, R. Burgmann, A. Rigo, D. Massonnet, and R. Reilinger (2002), Estimating slip distribution for the Izmit mainshock from coseismic GPS and INSAR measurements, *Bull. Seismol. Soc. Am.*, *92*, 138–160.

Flesch, L. M., W. E. Holt, A. J. Haines, and B. Shen-Tu (2000), Dynamics of the Pacific–North American plate boundary in the western United States, *Science*, *287*, 834–836.

Flesch, L. M., A. J. Haines, and W. E. Holt (2001), Dynamics of the India-Eurasia collision zone, *J. Geophys. Res.*, *106*, 16,435–16,460.

Gordon, R. G., and S. Stein (1992), Global tectonics and space geodesy, *Science*, *256*, 333–342.

Gordon, R. G., D. F. Argus, and M. B. Heflin (1999), Revised estimate of the angular velocity of India relative to Eurasia, *Eos Trans. AGU*, *80*(46), Fall Meet. Suppl., F273.

Hetland, E. A., and B. H. Hager (2003), Postseismic relaxation across the Central Nevada Seismic Belt, *J. Geophys. Res.*, *108*(B8), 2394, doi:10.1029/2002JB002257.

Le Pichon, X., N. Chamot-Rooke, S. Lallemant, R. Noomen, and G. Veis (1995), Geodetic determination of the kinematics of central Greece with respect to Europe, *J. Geophys. Res.*, *100*, 12,675–12,690.

McCaffrey, R. (2005), Block kinematics of the Pacific–North America plate boundary in the southwestern United States from inversion of GPS, seismological, and geologic data, *J. Geophys. Res.*, *110*, B07401, doi:10.1029/2004JB003307.

McClusky, S., et al. (2000), Global Positioning System constraints on plate kinematics and dynamics in the eastern Mediterranean and Caucasus, *J. Geophys. Res.*, *105*, 5695–5719.

McKenzie, D. (1990), Spinning continents, *Nature*, *344*, 109–110.

Meade, B. J. (2007), Mechanics of the India-Eurasia collision zone, *Geology*, in press.

Meade, B. J., and B. H. Hager (2005), Block models of crustal deformation in southern California constrained by GPS measurements, *J. Geophys. Res.*, *110*, B03403, doi:10.1029/2004JB003209.

Meyer, B., P. Tapponnier, L. Bourjot, F. Metivier, Y. Gaudemer, G. Peltzer, S. Guo, and Z. Chen (1998), Crustal thickening in Gansu-Xinghai, lithospheric mantle subduction, and oblique, strike-slip controlled growth of the Tibetan Plateau, *Geophys. J. Int.*, *135*, 1–47.

Molnar, P., and H. Lyon-Caen (1989), Fault plane solutions of earthquakes and the active tectonics of the Tibetan Plateau and its margins, *Geophys. J. Int.*, *99*, 123–153.

Molnar, P., and P. Tapponnier (1975), Cenozoic tectonics of Asia: Effects of continental collision, *Science*, *189*, 419–425.

Nyst, M., and W. Thatcher (2004), New constraints on the active tectonic deformation of the Aegean, *J. Geophys. Res.*, *109*, B11406, doi:10.1029/2003JB002830.

Peltzer, G., and F. Saucier (1996), Present-day kinematics of Asia derived from geologic fault rates, *J. Geophys. Res.*, *101*, 27,943–27,956.

Peltzer, G., and P. Tapponnier (1988), Formation and evolution of strike-slip faults, rifts, and basins during the India-Asia collision: An experimental approach, *J. Geophys. Res.*, *93*, 15,085–15,117.

Reigber, C., et al. (2001), New space geodetic constraints on the distribution of deformation in central Asia, *Earth Planet. Sci. Lett.*, *191*, 157–165.

Replumaz, A., and P. Tapponnier (2003), Reconstruction of the deformed collision zone between India and Asia by backward motion of lithospheric blocks, *J. Geophys. Res.*, *108*(B6), 2285, doi:10.1029/2001JB000661.

Royden, L. H., B. C. Burchfiel, R. W. King, E. Wang, Z. Chen, and L. Yuping (1997), Surface deformation and lower crustal flow in eastern Tibet, *Science*, *276*, 788–790.

Ryerson, F. J., P. Tapponnier, R. C. Finkel, A.-S. Meriaux, J. Van der Woerd, C. Lassiere, M.-L. Chevalier, X. Xiwei, and L. Harbing (2006), Applications of morphochronology to the active tectonics of Tibet, *Spec. Pap. Geol. Soc.*, *415*.

Sella, G. F., T. H. Dixon, and A. Mao (2002), REVEL: A model for recent plate motion velocities from space geodesy, *J. Geophys. Res.*, *107*(B4), 2081, doi:10.1029/2000JB000033.

Shen, Z.-K., J. Lü, M. Wang, and R. Bürgmann (2005), Contemporary crustal deformation around the southeast borderland of the Tibetan Plateau, *J. Geophys. Res.*, *110*, B11409, doi:10.1029/2004JB003421.

Tapponnier, P., Z. Xu, F. Roger, B. Meyer, N. Arnaud, G. Wittlinger, and J. Yang (2001), Oblique step-wise growth of the Tibetan Plateau, *Science*, *294*, 1671–1677.

Thatcher, W. (1983), Nonlinear strain buildup and the earthquake deformation cycle on the San Andreas fault, *J. Geophys. Res.*, *88*, 5893–5902.

Thatcher, W. (1995), Microplate versus continuum descriptions of active tectonic deformation, *J. Geophys. Res.*, *100*, 3885–3894.

Thatcher, W., and J. B. Rundle (1984), A viscoelastic coupling model for the cyclic deformation due to periodically repeated earthquakes at subduction zones, *J. Geophys. Res.*, *89*, 7631–7640.

Thatcher, W., G. R. Foulger, B. R. Julian, J. Svarc, E. Quilty, and G. W. Bawden (1999), Present day deformation across the Basin and Range Province, western United States, *Science*, *283*, 1714–1718.

Van der Woerd, J., X. Xiwei, L. Haibing, P. Tapponnier, B. Meyer, F. J. Ryerson, A.-S. Meriaux, and X. Zhiqin (2001), Rapid active thrusting along the northwestern range front of the Tanghe Nan Shan (western Gansu, China), *J. Geophys. Res.*, *106*, 30,475–30,504.

Vilotte, J. P., M. Dagnieres, and R. Madariaga (1982), Numerical modeling of interplate deformation: Simple mechanical models of continental collision, *J. Geophys. Res.*, *87*, 10,709–10,728.

Wallace, K., G. Yin, and R. Bilham (2004), Inescapable slow slip on the Altyn Tagh fault, *Geophys. Res. Lett.*, *31*, L09613, doi:10.1029/2004GL019724.

Wallace, L. M., J. Beavan, R. McCaffrey, and D. Darby (2004), Subduction zone coupling and tectonic block rotations in the North Island, New Zealand, *J. Geophys. Res.*, *109*, B12406, doi:10.1029/2004JB003241.

Wang, E., and B. C. Burchfiel (2004), Cenozoic right-lateral movement along the Wenquan fault and associated deformation: Implications for the kinematic history of the Qaidam Basin, northeastern Tibetan Plateau, *Int. Geol. Rev.*, *46*, 861–879.

Wang, E., B. C. Burchfiel, L. H. Royden, L. Chen, J. Chen, and W. Li (1998), Late Cenozoic Xianshuihe-Xiaojiang and Red River fault systems of southwestern Sichuan and central Yunnan, *Geol. Soc. Am. Spec. Pap.*, *327*, 109 pp.

Wang, Q., et al. (2001), Present-day crustal deformation of China constrained by Global Positioning System measurements, *Science*, *294*, 574–577.

Wright, T., B. Parsons, P. England, and E. Fielding (2004), InSAR observations of low slip rates on the major faults of western Tibet, *Science*, *305*, 236–239.

Yin, A., and M. T. Harrison (2000), Geological evolution of the Himalayan-Tibetan orogen, *Annu. Rev. Earth Planet. Sci.*, *28*, 211–280.

Zhang, P.-Z., B. C. Burchfiel, P. Molnar, W. Zhang, D. Ziao, Q. Deng, L. Royden, and F. Song (1990), Late Cenozoic tectonic evolution of the Ningxia-Hui Autonomous Region, China, *Geol. Soc. Am. Bull.*, *102*, 1484–1498.

Zhang, P.-Z., et al. (2004), Continuous deformation of the Tibetan Plateau from global positioning system data, *Geology*, *32*, 809–812, doi:10.1130/G20554.1.

Zhao, W.-L., and W.J. Morgan (1987), Injection of Indian crust into Tibetan lower crust: A two-dimensional finite element model study, *Tectonics*, *6*, 489–504.

W. Thatcher, U.S. Geological Survey, 345 Middlefield Road, MS 977, Menlo Park, CA 94025, USA. (thatcher@usgs.gov)